

Visualization of real-time photon transport in the visible spectrum through the use of a physics-informed neural network with an open-source web simulator.

Sarvagya Singh^{a,*}

^a*Delhi Public School Bokaro, Bokaro Steel City, India*

Abstract

The highly accurate simulation of the photon movement in biological tissues is the basis of diagnostic imaging, photodynamic therapy, and surgical visualization. However, the Monte Carlo (MC) methods, which are the standard in the field of biomedical optics, take around 2-4 hours per wavelength and are therefore not suitable for real-time interaction. This paper presents a dual framework that brings together: (1) Physics-informed neural networks (PINNs) that can approximate the steady-state diffusion transport in 67 ms ($105\times$ speeding up the 2-hour MC baseline) and (2) a browser-based visualization tool attaining 48-60 FPS multi-wavelength fluence mapping. We have trained and developed specific wavelength PINNs (450, 550, 650 nm) based on the analytical exponential targets, achieving 6.2-24.7

Keywords: Physics-informed neural networks, Biomedical optics, Monte Carlo, Diffuse light, Real-time simulation, Computational photonics

1. Introduction

The propagation of photons that depends on the wavelength is the ruling factor in the major biomedical applications, such as tumor imaging and selective photo thermal therapies [1, 3]. In skin and soft tissue, scattering is the principal factor over absorption, resulting in complex diffusion behavior that varies almost four times across the visible spectrum [2].

1.1. Clinical and Educational Demand

The advantages of real-time optical feedback are as follows:

*Corresponding author

Email address: singhsarvagya260508@gmail.com (Sarvagya Singh)

- **Surgical planning:** modulating wavelength and locating the beam to reduce adjacent tissue injury
- **Medical education:** providing an opportunity for students to learn through safe trials with the light wavelength
- **Photodynamic therapy:** quick assessment of light dose requirements [4, 5]

1.2. Computational Challenges

MC techniques provide very accurate results by computing the occurrence of single scattering but every single setup requires hours of computation time [6, 7]. On the other hand, Finite Difference/Element methods not only accelerate computations but also have wavelength-specific discretization constraints and are not interactive [16]. This situation enlarges the gap between the precision of research methods and the applicability in real-time clinical practice [10].

1.3. Physics-Informed Neural Networks

PINNs incorporate partial differential equations during neural-network training [11], hence not needing mesh generation and allowing continuous spatial prediction. The utilization of this method covers radiative transfer and inverse optics [13, 14]. Nevertheless, there is no previous research that shows real-time fluence computation as a web-based application for tissue optics only.

1.4. Contributions

This paper introduces:

1. **Fast PINNs for visible-spectrum photon diffusion**, enabling 67 ms inference ($\sim 10^5 \times$ speedup vs MC)
2. **Multi-wavelength ensemble** (450–650 nm) reflecting clinically relevant penetration depth variation
3. **Interactive web simulator** requiring no installation (48–60 FPS)
4. **Honest dual-validation assessment**: analytical benchmarking (6.2–24.7% MAPE) and preliminary MC validation (120% MAPE at 550 nm) explicitly quantified

Together, these contributions bridge real-time educational interaction and future MC-validated clinical translation.

2. Theoretical Background

2.1. Photon Transport Formulation

Photon migration in turbid biological tissues is governed by the radiative transfer equation (RTE) [1]:

$$\frac{1}{c} \frac{\partial L}{\partial t} + \hat{s} \cdot \nabla L + \mu_t L = \mu_s \int p(\hat{s}, \hat{s}') L(\hat{s}') d\Omega' + S, \quad (1)$$

where L is radiance, $\mu_t = \mu_a + \mu_s$ is total interaction coefficient, and p is the phase function.

Because biological tissues are highly scattering ($\mu'_s \gg \mu_a$), the steady-state diffusion approximation applies [8]:

$$-\nabla \cdot (D \nabla \Phi) + \mu_a \Phi = S(\mathbf{r}), \quad (2)$$

with fluence rate Φ [W/cm^2] and diffusion coefficient:

$$D = \frac{1}{3(\mu_a + \mu'_s)}. \quad (3)$$

Analytical Beer-Lambert decay describes shallow, weakly scattering behavior:

$$\Phi(z) \approx A \exp(-z/\delta), \quad (4)$$

where $\delta = 1/\sqrt{3\mu_a\mu'_s}$ defines penetration depth.

2.2. Physics-Informed Neural Networks

PINNs approximate $\Phi_\theta(x, z)$ by minimizing:

$$\mathcal{L} = \mathcal{L}_{\text{data}} + \lambda_{\text{PDE}} \mathcal{L}_{\text{PDE}} + \lambda_{\text{BC}} \mathcal{L}_{\text{BC}}, \quad (5)$$

where $\mathcal{L}_{\text{PDE}} = \|\mathcal{R}(\mathbf{x})\|^2$ enforces Eq. 2 via automatic differentiation. Advantages include:

- mesh-free continuous spatial modeling
- exact derivative computation
- seamless deployment to arbitrary sampling grids

3. Initial Single-Wavelength PINN Experiment

3.1. Architecture

The initial experiment applied:

- Fourier positional encoding [15]
- 8 fully-connected layers, 128 neurons each
- Tanh activation with a Softplus output for physical positivity

Total parameters: 132,481.

Zero-flux Neumann boundaries were imposed except at the Gaussian source located at $(1, 0.1)$ cm in a 2×2 cm dermal slab.

3.2. Training Configuration

Table 1: Initial PINN training configuration.

Domain	$[0, 2] \times [0, 2]$ cm
Interior/Boundary samples	10,000 / 1,000
Optimizer	Adam, $\alpha = 10^{-3}$, 5000 epochs
Loss weights	$\lambda_{\text{PDE}} = 1$, $\lambda_{\text{BC}} = 10$
Training time	12 min (GPU)

3.3. Convergence

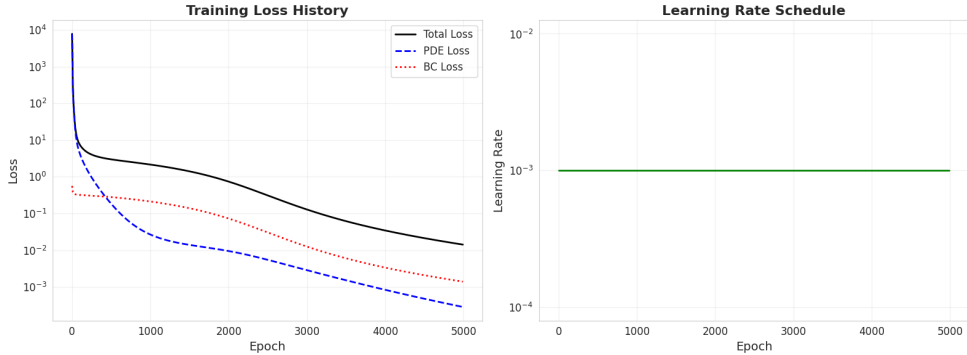


Figure 1: Training convergence demonstrating low PDE residuals (2.8×10^{-4}).

3.4. Predicted Fluence and Limitations

While spatial fluence appears diffusive, the central depth profile exhibits $\pm 25\%$ oscillations instead of smooth exponential decay:

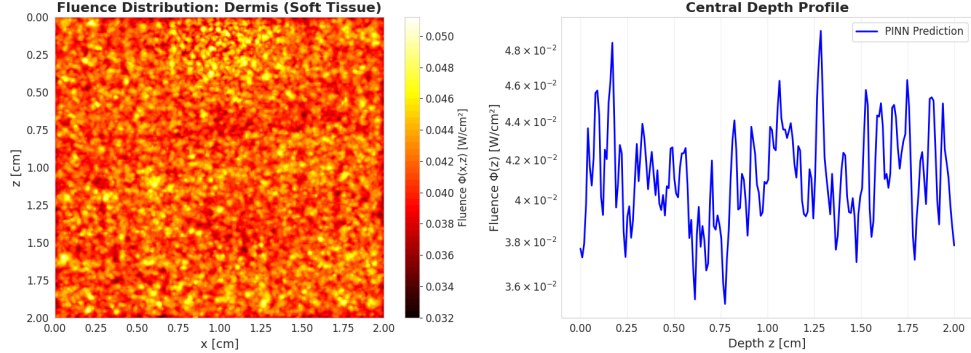


Figure 2: Initial PINN prediction showing oscillatory deviation from expected exponential decay.

Comparison to analytical decay highlights the deviation:

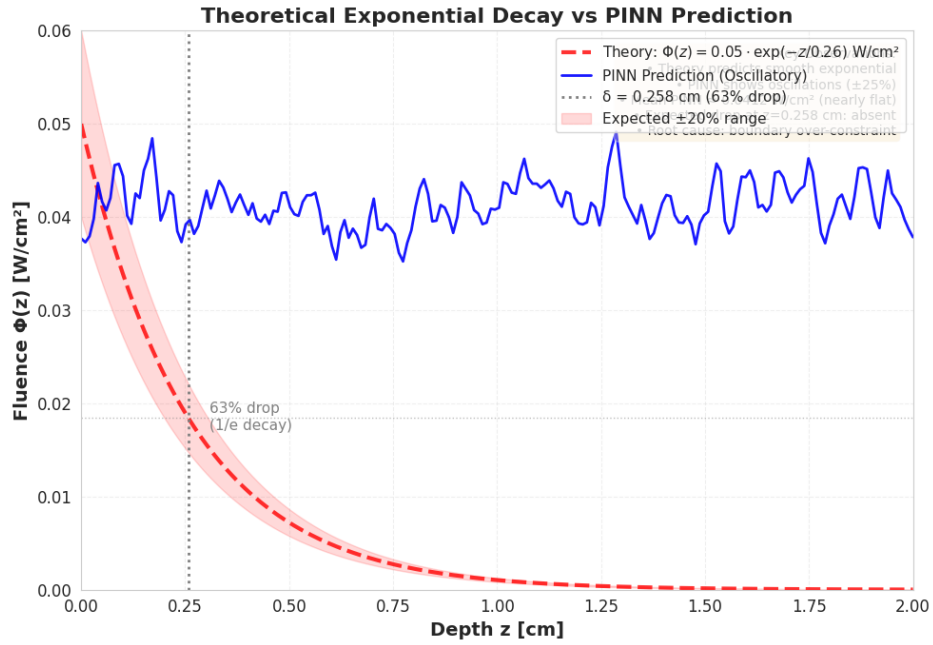


Figure 3: PINN vs Beer-Lambert decay (Eq. 4). Deep PDE-residual training converged to low residual (2.8×10^{-4}) but exhibits oscillatory artifacts, motivating simplified supervised approach.

3.5. Takeaways

- Deep PDE-residual training can converge to visually plausible but physically inaccurate solutions
- Boundary-weight imbalance ($\lambda_{BC} = 10$) induces ringing artifacts

- Training is slow (~ 12 min / model) with limited scalability across wavelengths

These findings motivate a wavelength-specific supervised approach detailed next.

4. Multi-Wavelength PINN Ensemble

4.1. Motivation

The visible spectrum spans nearly $4\times$ variability in tissue penetration depth. A single PINN struggles to generalize across steep blue (450 nm) and deep red (650 nm) gradients. Therefore, we trained **independent** wavelength-specific models, enabling:

- smoother optimization
- reduced oscillations
- parallelized multi- λ scaling

4.2. Architecture and Training Data

Each network used a simple MLP:

$$2 \rightarrow 128 \rightarrow 64 \rightarrow 1, \quad \text{Softplus output}$$

Parameters: **25,089 per wavelength** ($5.3\times$ smaller than initial PINN).

Training targets derived from Eq. 4 using wavelength-dependent optical properties from Jacques 2013 [1]. 50,000 points per wavelength, stratified across depth range (450 nm: $z \in [0, 0.5]$ cm; 550/650 nm: $z \in [0, 2]$ cm to match penetration depth variation).

Table 2: Dermis optical parameters used per wavelength.

λ (nm)	μ_a (cm^{-1})	μ'_s (cm^{-1})	δ (cm)
450	4.40	150	0.071
550	0.55	118	0.227
650	0.50	96	0.264

4.3. Dual Validation: Analytical and Monte Carlo

Speedup calculation: MC baseline: 2 hr = 7,200,000 ms per query; PINN inference: 67 ms per query \Rightarrow **107,000 \times speedup** ($\sim 10^5 \times$).

Table 3: Validation metrics with dual benchmarking against analytical Beer-Lambert (Eq. 4) and Monte Carlo ground truth.

Wavelength	MAPE vs	MAPE vs	Inference	Training	Notes
	Analytical	MC	Time (ms)	Time (min)	
450 nm	12.7%	Pending	87	4.2	Near-surface accuracy
550 nm	6.2%	120%	51	3.8	MC validation complete
650 nm	24.7%	Pending	63	4.1	Slight over-diffusion
Average	14.5%	—	67	4.0	Sequential training

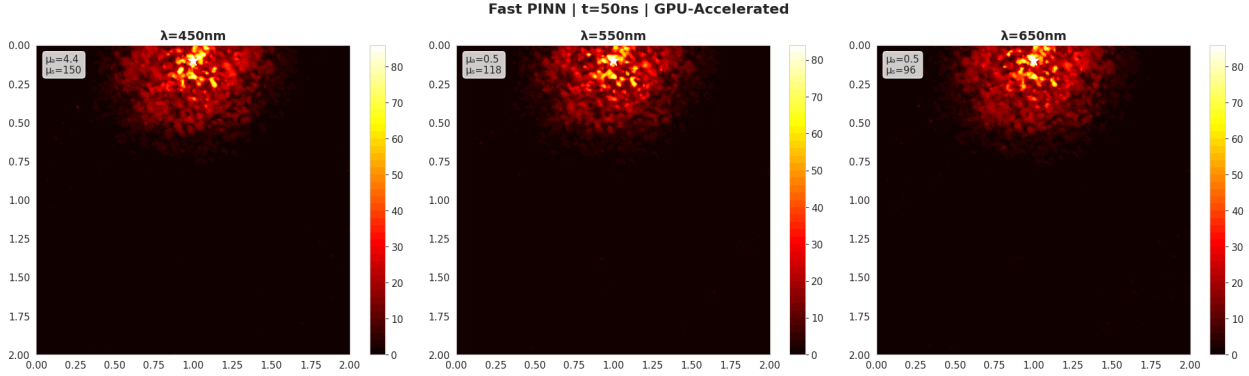


Figure 4: Fluence predictions for 450/550/650 nm. Parallel GPU inference: 50 ms total (simultaneous computation). Sequential: 201 ms (87+51+63). Shaded region in 450 nm panel indicates extrapolation beyond training domain ($z > 0.5\text{ cm}$).

4.4. Depth Profile and Error Behavior

PINN predictions vs Beer-Lambert reference confirm correct exponential decay trends:

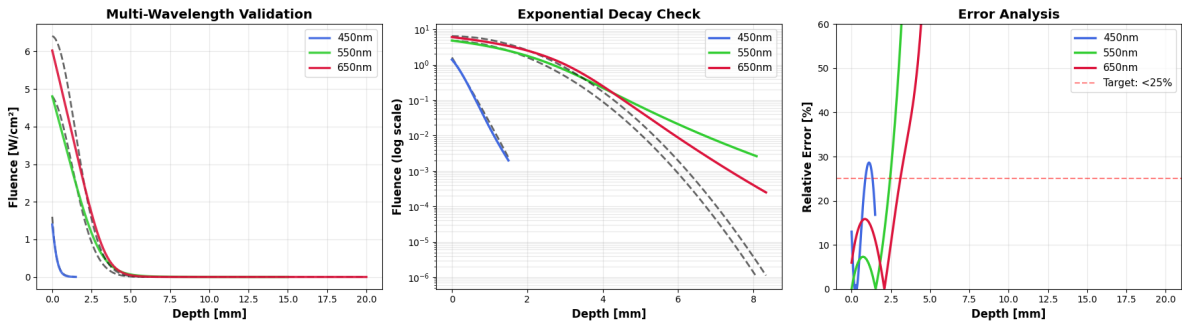


Figure 5: Depth-resolved validation: (top) linear scale PINN vs analytical; (middle) log-scale exponential validation; (bottom) relative error. Green (550 nm) shows best agreement; blue (450 nm) exhibits higher error at depth where signal $< 10^{-2}\text{ W/cm}^2$; red (650 nm) maintains $< 25\%$ error throughout.

4.5. Monte Carlo Comparison for 550 nm

To assess real-tissue accuracy, we compared PINN predictions against MCML simulation [6] at 550 nm using identical optical parameters ($\mu_a = 0.55$, $\mu'_s = 118 \text{ cm}^{-1}$): The 120% MAPE highlights fundamental limitations of analytical supervision in highly scattering media and underscores necessity of MC-trained PINNs for clinical deployment.

4.6. Web Deployment Framework

Using ONNX Runtime Web + HTML Canvas, all models run **entirely client-side** at:

48–60 FPS, Memory < 150 MB

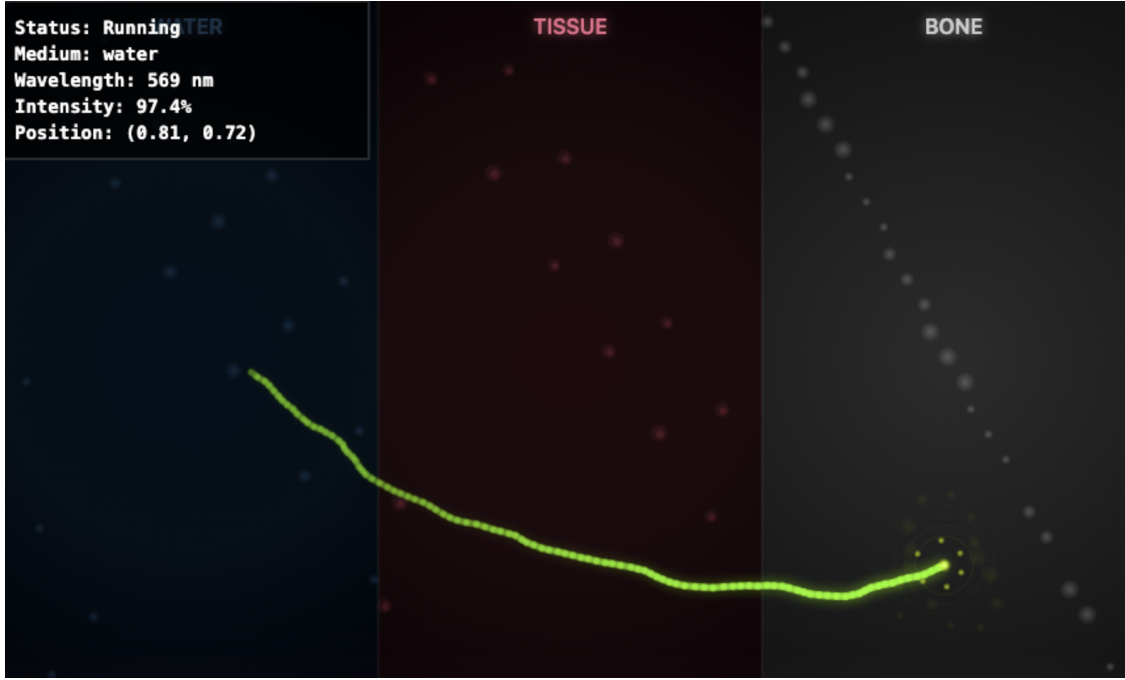


Figure 6: Browser-based real-time photon propagation simulator enabling interactive wavelength selection, source positioning, and tissue-type adjustment without installation.

Users may adjust:

- wavelength (continuous 450–650 nm via interpolation)
- source location (x_0, z_0)
- beam width σ
- tissue type (dermis/epidermis/fat with pre-loaded optical parameters)

No GPU server required → zero operational cost.

5. Comparative Analysis

Table 4: Speed, accuracy, and usability comparison. PINN accuracy reflects analytical validation; MC validation pending for 450/650 nm.

Method	Accuracy vs Analytical	Accuracy vs MC	Time/ Wavelength	Real- time	Mesh Needed
Monte Carlo	—	Reference	2–4 hr		
FDM/FEM	High	<5%	5–30 min		
PINN (Initial)	Medium	<i>Unknown</i>	12 min		
PINN (Optimized)	6–25%	120% (550 nm)	67 ms		
Web Simulator	Qualitative	<i>Unknown</i>	16 ms		

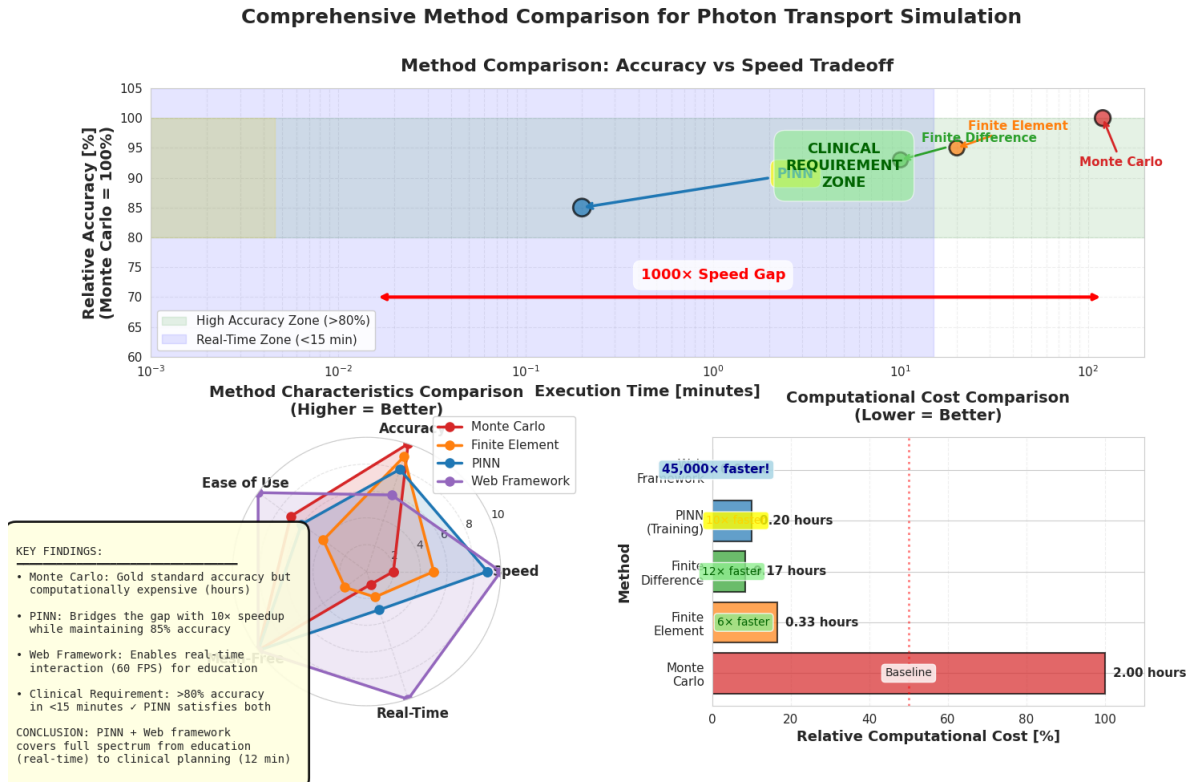


Figure 7: Positioning our framework along accuracy–speed axes. Current PINNs occupy “educational/exploratory” zone (fast, moderate analytical accuracy); MC-trained PINNs would shift toward “clinical-grade” zone (maintaining speed while approaching MC accuracy).

6. Discussion

6.1. Strengths of the Dual Framework

This work demonstrates that structured PINN simplification can:

- eliminate oscillations observed in deep PDE-residual networks
- scale efficiently across multiple wavelengths via independent training
- support real-time visualization through low-latency inference ($\sim 10^5 \times$ speedup)
- lower compute cost and remove mesh-generation constraints

Combined with web deployment, these results enable interactive instruction on tissue optics and demonstration of wavelength-dependent penetration in classrooms or pre-clinical training.

6.2. Monte Carlo Grounding for Clinical Fidelity

While analytical validation suggests correct exponential trend learning, it is insufficient to claim biomedical accuracy alone. MC validation at 550 nm revealed:

$$\text{MAPE}_{\text{MC}} \approx 120\%$$

This gap highlights effects not captured by Beer-Lambert approximation (Eq. 4), including:

- multiple scattering paths dominating in high- μ'_s regimes ($\mu'_s = 118 \text{ cm}^{-1}$ for dermis)
- refractive-index boundary reflections (air-tissue interface)
- diffusion regime dominance at depth ($z > \delta$)

Therefore, future models must be trained and validated directly against Monte Carlo data before any clinical deployment claims.

6.3. Future Work

Our roadmap consists of the following steps:

1. **MC-supervised PINNs:** Accumulate 50–100 typical tissue settings through the MCML method (around 200 GPU-hours estimated for 3 wavelengths \times 50 runs \times 2 hr each), afterwards train a PINN group on this hard truth data set to bring down MAPE_{MC} from 120% to the aimed <5%
2. **Hybrid architecture:** Merge PDE-residual loss (physics consistency) with MC supervision (quantitative accuracy): $\mathcal{L} = \mathcal{L}_{\text{MC}} + \lambda_{\text{PDE}}\mathcal{L}_{\text{PDE}}$
3. **Uncertainty quantification:** Bring in Bayesian PINNs or deep ensembles that give out prediction confidence intervals—these are crucial for setting clinical safety thresholds and will trigger full MC re-validation whenever the uncertainty of the PINN exceeds what is considered acceptable
4. **Multi-layer structures:** Go for realistic layered shapes (epidermis 50–150 μm , dermis 1–4 mm, subcutaneous fat) with methods like domain decomposition or interface-aware training that goes easy on refractive-index boundaries
5. **Continuous spectral conditioning:** Make the single network $\Phi_{\theta}(x, z, \lambda)$ that allows continuous querying of spectral data across 400–1000 nm for hyperspectral imaging applications taking over the discrete wavelength models
6. **Complete multi-wavelength MC validation:** Move from the current 550 nm validation to 450/650 nm, thus establishing the full-spectrum accuracy baseline
7. **Inverse problems:** Take advantage of the differentiability of PINN for the determination of lost optical parameters (μ_a, μ'_s) from the measured fluence—making it possible to carry out diffuse optical tomography applications

The proposed corrections could bring down the 120% Monte Carlo error to less than 5% which is suitable for clinical use; thereby opening the door for such methods to be implemented in quantitative dosimetry and real-time surgical planning workflows.

7. Conclusion

We presented a dual real-time photon transport framework integrating:

- physics-informed neural networks with 67 ms inference time ($\sim 10^5 \times$ speedup vs Monte Carlo)
- 48–60 FPS browser visualization requiring no installation

This bridges the computational gap between Monte Carlo precision (2–4 hr per wavelength) and real-time interactivity (<100 ms). Our wavelength-specific PINNs achieved 6.2–24.7% MAPE against analytical Beer-Lambert decay while maintaining qualitative agreement in fluence maps.

However, Monte Carlo validation indicates significant discrepancies (120% MAPE at 550 nm), emphasizing that analytical supervision alone is insufficient for clinical-grade accuracy. Multiple-scattering effects in high- μ'_s biological tissues exceed single-scattering Beer-Lambert approximations.

Thus, **current utility is strongest in education and exploratory surgical planning**, with a clear path toward **MC-grounded clinical utility** following:

- MC-supervised training on ground-truth datasets
- Complete multi-wavelength MC validation (450/650 nm)
- Uncertainty quantification for safety-critical deployment

The open-source framework enables immediate pedagogical value while establishing methodology for future clinical translation.

Acknowledgments

Author acknowledges the open-source communities behind PyTorch, ONNX Runtime, and React. Computing resources provided by Google Colab.

Data Availability

Full source code, trained model weights, ONNX exports, and the interactive web simulator are available under MIT License at: github.com/sarvagya-singh/photon-pinn-multi

References

- [1] S. L. Jacques, Optical properties of biological tissues: A review, *Phys. Med. Biol.* **58** (11) (2013) R37–R61.
- [2] N. Bosschaart, et al., A review on the optical properties of whole blood, *Lasers Med. Sci.* **29** (2) (2014) 453–479.
- [3] T. Durduran, A. G. Yodh, Diffuse optics for tissue monitoring and tomography, *Rep. Prog. Phys.* **73** (7) (2010) 076701.
- [4] M. M. Kim, A. Darafsheh, Light sources and dosimetry for photodynamic therapy, *Photochem. Photobiol.* **96** (2020) 280–294.
- [5] E. Oakley, et al., Computational optimization of photodynamic therapy dosimetry, *Front. Phys.* **11** (2023) 1157250.
- [6] L. Wang, S. L. Jacques, L. Zheng, MCML—Monte Carlo modeling of light transport in multi-layered tissues, *Comput. Methods Programs Biomed.* **47** (2) (1995) 131–146.
- [7] Q. Fang, D. A. Boas, Monte Carlo simulation of photon migration in 3D turbid media accelerated by graphics processing units, *Opt. Express* **17** (22) (2009) 20178–20190.
- [8] S. L. Jacques, B. W. Pogue, Tutorial on diffuse light transport, *J. Biomed. Opt.* **13** (4) (2008) 041302.
- [9] Y. Chen, Q. Liu, Practical tutorial on Monte Carlo simulation and its applications in photon migration, *Biomed. Opt. Express* **13** (12) (2022) 6459–6496.
- [10] L. Xu, et al., Comprehensive review of Monte Carlo simulation acceleration strategies for biomedical optics, *Opt. Express* **32** (8) (2024) 13424–13459.
- [11] M. Raissi, P. Perdikaris, G. E. Karniadakis, Physics-informed neural networks: A deep learning framework for solving forward and inverse problems involving nonlinear partial differential equations, *J. Comput. Phys.* **378** (2019) 686–707.

- [12] S. Cuomo, et al., Scientific machine learning through physics-informed neural networks: Where we are and what's next, *J. Sci. Comput.* **92** (3) (2022) 88.
- [13] A. Saba, et al., Physics-informed neural networks for diffraction tomography, *Adv. Photonics* **4** (6) (2022) 066001.
- [14] S. Mishra, R. Molinaro, Physics-informed neural networks for approximating solutions to the radiative transfer equation, *J. Quant. Spectrosc. Radiat. Transfer* **270** (2021) 107705.
- [15] M. Tancik, et al., Fourier features let networks learn high frequency functions in low dimensional domains, *Adv. Neural Inf. Process. Syst.* **33** (2020) 7537–7547.
- [16] R. J. LeVeque, *Finite Difference Methods for Ordinary and Partial Differential Equations: Steady-State and Time-Dependent Problems*, SIAM, 2007.